The dynamic behavior of gas hydrate dissociation by heating in tight sandy reservoirs A molecular dynamics simulation study

Fang, Bin; Ning, Fulong; Ou, Wenjia; Wang, Dongdong; Zhang, Zhun; Yu, Yanjiang; Lu, Hongfeng; Wu, Jianyang; Vlugt, Thijs J.H.

DOI
10.1016/j.fuel.2019.116106

Publication date
2019

Document Version
Accepted author manuscript

Published in
Fuel

Citation (APA)
Fang, B., Ning, F., Ou, W., Wang, D., Zhang, Z., Yu, Y., Lu, H., Wu, J., & Vlugt, T. J. H. (2019). The dynamic behavior of gas hydrate dissociation by heating in tight sandy reservoirs: A molecular dynamics simulation study. *Fuel*, *258*, Article 116106. https://doi.org/10.1016/j.fuel.2019.116106

The Dynamic Behavior of Gas Hydrate Dissociation by Heating in Tight Sandy Reservoirs: A Molecular Dynamics Simulation Study

Bin Fang[1], Fulong Ning[1,2]*, Wenjia Ou[1], Dongdong Wang[1], Zhun Zhang[1,2], Yanjiang Yu[3], Hongfeng Lu[3], Jianyang Wu[4], Thijs J. H. Vlugt[5]

1 National Center for International Research on Deep Earth Drilling and Resource Development, Faculty of Engineering, China University of Geosciences, Wuhan, Hubei 430074, China

2 Laboratory for Marine Mineral Resources, Qingdao National Laboratory for Marine Science and Technology, Qingdao 266237, China

3 Guangzhou Marine Geological Survey, Ministry of Land and Resources, Guangzhou 510760, China

4 Department of Physics, Research Institute for Biomimetics and Soft Matter, Jiujiang Research Institute and Fujian Provincial Key Laboratory for Soft Functional Materials Research, Xiamen University, Xiamen 361005, PR China

5 Process and Energy Department, Delft University of Technology, Leeghwaterstraat 39, 2628CB Delft, The Netherlands

Email address:

fangbin126@cug.edu.cn

wenjiaou1985@163.com

wdd8597@163.com

20121003712@cug.edu.cn

yuyanjiang2004@163.com

gmgslhf@126.com

jianyang@xmu.edu.cn

t.j.h.vlugt@tudelft.nl

*To whom correspondence should be addressed: nflzx@cug.edu.cn

Abstract

Knowledge on the kinetics of gas hydrate dissociation in microporous sediments is very important for developing safe and efficient approaches to gas recovery from natural gas hydrate (NGH) deposits. Herein, molecular dynamics (MD) simulations are used to study the dissociation kinetics in microporous sediments. The hydrate phase occupies a confined sandy nanopore formed by two hydroxylated silica surfaces with a buffering water layer between the hydrate and silica phase, meanwhile, this system is in contact with the bulk phase outside the pore. The hydrates in this sediment system dissociate layer-by-layer in a shrinking core manner. The released methane molecules aggregate and eventually evolve into nanobubbles, most of which are spherical cap-shaped on the hydroxylated silica surfaces. At high initial temperatures, a faster decomposition of the hydrate phase is observed, however, fewer methane molecules migrate to the bulk phase from the pore phase. These phenomena may occur because more methane molecules are released from the hydrate phase and facilitate the formation of nanobubbles with large heat injection; these nanobubbles can stably adsorb on the surface of silica and capture the surrounding methane molecules, thereby decreasing the number of methane molecules in the water phase. In addition, the injection speed of heat flow should be significantly increased at high dissociation temperatures when using the thermal stimulation method to extract gas from hydrates in tight sediments. This study provides molecular level insight into the kinetic mechanism of hydrate dissociation and theoretical guidance for gas production by thermal injection from sediments with low permeabilities.

Keywords: methane hydrate; molecular simulation; dissociation kinetics; nanobubbles; tight sandy sediments; heat injection;

1. Introduction

Clathrate hydrates are crystalline ice-like solids in which certain compounds (hydrate formers) stabilize the polyhedral cages formed by hydrogen-bonded (H-bonded) concomitant water molecules [1]. If a hydrate former exists in the state of a gas, such as methane, the clathrate hydrates are called gas (methane) hydrates. This unconventional source of methane in natural gas hydrates (NGHs) can potentially serve as an energy source for the future, instead of fossil fuels approaching depletion with gradually increasing energy consumption. NGHs have been identified as presently containing twice the energy stored in all other fossil fuel deposits [2, 3]. NGHs play an important role in energy production as a methane resource stored in hydrates and as a safety and environmental problem in hydrocarbon production. Currently, natural gas production from NGHs has attracted much attention, and certain countries have been testing production from permafrost regions and deep oceans where NGHs often occur [3]. It is well known that marine gas hydrates account for more than 90% of the global NGHs; thus far, depressurization, thermal stimulation, chemical inhibitor injection, guest molecule exchange and combination technologies have been proposed as gas extraction techniques from marine sediments [4]. To accelerate the process of industrial production, knowledge of the kinetics of hydrate dissociation is of crucial importance to understanding gas/water production across a range of conditions, especially in marine sediments.

Marine NGHs are thought to mainly exist in natural porous environments, especially occurring in low-permeability, unconsolidated muds reaching the micro- or nano level [5]. Nevertheless, gas production in these reservoirs is a complex process involving kinetics, thermodynamics, geoengineering, etc. It is essential to simulate natural gas production from different reservoirs systematically in the laboratory before natural gas production field tests. However, one of the key factors for this approach is that the kinetics of dissociation in sediments with low permeabilities can hardly be observed directly via macroscopic numerical and experimental simulation tests.

Although many studies have focused on the dissociation processes of hydrates [6-8], the fundamental kinetics of hydrate dissociation in a low-permeability porous environment are still unclear, which is one of the core issues of the safe and efficient gas hydrate extraction in marine sediments. To identify and quantify such molecular mechanisms, molecular dynamics (MD) simulations have been used to investigate the static and dynamic properties of gas hydrates in sediments. Previous studies focused on hydrate phase behavior [9-11], nucleation and growth [12-24], transport properties [25, 26], and chemical inhibition [27-37]. In addition, the kinetics of methane hydrates dissociation within the water phase have been widely studied using MD simulation and discussed in detail in previous studies [38-53]. The dissociation processes of NGHs is described as a two-step process: first, the enhanced diffusive behaviors of the host water

molecules in the hydrate crystals lead to unit cell size increases and distortions that ultimately break down the lattices, and second, methane molecules escape from these incomplete cages and aggregate.[38-40] The investigation of the effects of external factors on the hydrate dissociation kinetics process, such as the heat transfer [43, 52], sediment skeleton type [41, 46], hydrate type [44, 45, 49], and electrolyte solution [42, 47], is ongoing. The formation and evolution of nanobubbles during hydrate decomposition are important in determining the decomposition rate and understanding the gas-liquid phase flow behaviors, and it may be possible to control the dissociation process by suppressing or enhancing bubble formation caused by the solvation of other materials or surface structures of the container or other external factors [42, 48, 50, 51]. These dissociation simulations are usually performed by applying an MD thermostat at an overtemperature higher than the hydrate−water−gas equilibrium points in the water phase, while seldomly performed in the quartz sand nanopore phase. Therefore, the characteristics of flow, heat and mass transfer of the dissociation behaviors in these reservoirs are still not comprehensively recognized.

Based on the previous research results, we construct molecular models to describe gas hydrate dissociation in low-permeability sediments with different initial temperatures using MD simulations at adiabatic, constant energy, volume (NVE) conditions. In this work, the focus is on the understanding of the microscopic mechanisms and kinetics of dissociation by conventional heat stimulation at natural sediments conditions. In contrast to previous dissociation systems, in addition to the hydrate phase within the pore phase the bulk phase is considered in our simulations, which can provide heat consumption for hydrate dissociation and diffusion regions for mass transfer. The MD model is closer to the NGH dissociation environments in sediments. This work provides molecular insight into the mechanism of different initial temperatures influencing gas hydrate dissociation in low-permeability sediments. Our work lays a solid foundation for gas productivity evaluation and reservoir reconstruction based on dissociation knowledge; meanwhile, this research may also have strategic importance for alleviating energy shortages, controlling climate variations, and sustainable development.

2. Computational method

2.1 Simulation details

Here, we focus on the kinetic process of hydrate dissociation within the nanopores, which approximate to the geological setting where hydrate-bearing sediments are saturated with water and no free gas phase exists. The molecular model for the kinetics of hydrate dissociation in microporous sediments is shown in Fig. 1. The initial conformation can be divided into left and right moieties. The left moiety is the bulk water phase, and the other moiety is the hydrate phase between the two hydroxylated silica phases that act as two-dimensional pore walls. Additionally, a buffering water layer with a thickness of 5 Å is deployed

between the hydrate and silica due to the fact that the bound water on the surfaces of semimetal grains cannot be 100% converted into hydrate both in simulations and experiments, and this thin water layer could relieve the mismatch between hydrate and silica two solid lattices [54-60]. Therefore, the initial structure consists of 4 layers of hydrate/water/hydroxylated silica/ bulk water. To the best of our knowledge, this hydrate dissociation model at the molecular level is the closest to natural sedimentation environment.

Molecular simulations were performed using the Gromacs package version 2018 [61, 62]. The hydrate phase consisted of 3×6×14 cubic unit cells, and each unit cell was built as follows: the water oxygen atoms positions of the initial hydrate unit cell were obtained from X-ray crystallography, and the hydrogen atoms of water were inserted by adjusting the orientations to obey the Bernal-Fowler rule and minimize the potential energy and net unit cell dipole moment [63]. The methane molecules were placed at the center of the water polyhedral cages made up by the water hydrogen-bond networks, assuming that the methane molecules fully occupied the water cages; the lattice parameter of a unit cell is 12.03 Å [63]. We extracted the orthorhombic supercell for silica (quartz) from the crystallographic hexagonal unit cell of this substance available from the American Mineralogist Crystal Structure Database, which is the same as Bagherzadeh's work [64]. The constructed parameters were as follows: each wall of silica consisted of 7×1×31 unit cells, and the silicon atoms of edge sites are saturated with OH groups, which is in adjacent to the methane hydrate phase separated by a water layer. To remove the mismatch between the silica and hydrate crystal, we expanded the length in the x-direction of the silica crystal slab to be in accordance with that of hydrate crystal. The atoms of the silica slabs were kept frozen and constituted the immobile substrate throughout the simulations and therefore did not participate in heat transfer except the atoms of the OH group.

A total of 112089 atoms, including 33856 water and 2016 methane molecules, were present in the initial simulation box (with initial dimensions of 3.61x10.12x33.51 nm). The initial size of the simulation box along the x direction is the same for both the hydrate and silica crystal, consequently, it can produce about 0.17 nm difference in x direction length of the silica crystal. This small difference can be safely ignored in the simulation when compared with that of silica crystal (3.44 nm). The optimized potential for liquid simulations (OPLS) united-atom force field was used for methane [65]. Water was described by the SPC/E model [66]. and the potential developed by Lopes et al. was used for the silica atomic interactions [67]. The particle-mesh Ewald (PME) summation method was used to handle the long range electrostatic interactions [68]. The van der Waals interactions were calculated using the Lennard-Jones potential (for the unlike pairs of atoms, standard combination rules are utilized) with a cut-off distance of 1.2 nm. Newton's equation of motion was described by the leap-frog algorithm for integrating with a 1 fs time step [69]. To minimize the system energy and relax the molecules especially the water at the silica/water and hydrate/water interface, a conjugate gradient algorithm was used for energy minimization [70], Simulation

runs of 200 ps (NVT ensemble) were carried out for temperature equilibrium followed by 200 ps NPT simulations for the relaxation of the pressure. During the NPT simulation, the configuration volume is fluctuating due to the relaxed simulation cell. In practice, this fluctuation is small. The equilibrium temperatures were 292 K, 302 K, and 312 K, and the equilibrate pressure was 3 MPa. Temperature and pressure controls were implemented using velocity rescaling with a stochastic term [71] and Parrinello-Rahman extended-ensemble pressure coupling [72], respectively. Thermostat and barostat constants of 0.1 and 1.0 ps, respectively, were used in these simulations. A simulation time of 50 ns was used under the NVE ensemble with initial temperatures of 292 K, 302 K, and 312 K.

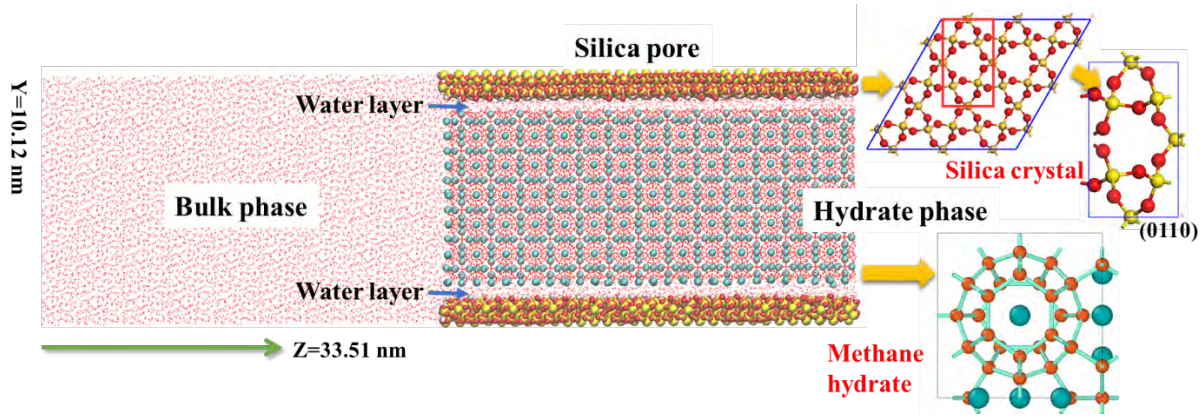

Fig. 1. Initial simulation configuration. Four phases are shown, including the bulk phase, silica pore phase and hydrate phase as well as the water layer. The right part presents the process of silica crystal construction and the cubic unit cell of silica, as well as the sI methane hydrate lattice. Si (yellow); O (red); H (white); C (cyan). The (0110) basal plane is hydroxylated.

2.2 Distinguished criteria

To determine which water and methane molecules belong to the hydrate phase during the dissociation, selection criteria are necessary. Generally, the water oxygen atoms can form the vertexes of tetrahedral element with four oxygen atoms of neighboring water in ice and hydrate phase, and the F_3 parameter is based on the 104.25° O-O-O angle arrangement which is quite different in liquid phase [73]. Therefore, the local states of the water molecules can be characterized by the F_3 order parameter proposed by Baez and Clancy [38] during the hydrate dissociation simulations. This algorithm can provide a deviation of the H-bonded network of water molecules in the solid state from standard tetrahedral structures:

$$F_{3,i} = \left\langle \left[\cos\theta_{jik} \left| \cos\theta_{jik} \right| + \cos^2 104.25 \right]^2 \right\rangle_{j,k} = \begin{cases} \sim 0.1 & \text{liquid water} \\ \sim 0.0 & \text{solid water (ice,hydrate)} \end{cases} \quad (1)$$

where θ_{jik} is the angle between triplets of oxygen atoms, and the ith atom is in the center, the j and k oxygen atoms are on either hand of atom i within a spherical shell with a radius of 3.5 Å (the first minimum in the radial distribution function of the O−O pairs of the water molecules in the liquid water phase). The

values of F_3 for disordered structures are larger than those for tetrahedral structures, such as clathrate hydrates. In our simulations, water molecules belong to the hydrate phase if F_3 is smaller than 0.05. Methane molecules can easily escape from the incomplete hydrate H-bonded cage when several host water molecules of this cage shed the intermolecular H-bond constrain. Therefore, we assume that a methane molecule remains in a polyhedral H-bonded cage of hydrate if the number of surrounding hydrate-phase ($F_3 < 0.05$ defined as above) water molecules within the first hydrate shell for the methane molecule (5.5 Å) is larger than 15 [74, 75].

3. Results and discussion

3.1 Kinetics of hydrate dissociation within the sandy nanopore

The methane hydrates in the simulations are fully occupied within the silica nanopore, and the methane hydrate dissociation process and nanobubble evolution over time, with the system at an initial temperature of 292 K, are used as examples. Six yz snapshots corresponding to different dissociation times are shown in Fig. 2. By computing the local order parameter F_3, we can distinguish the water molecules belonging to the hydrate phase or not. The hydrate cluster is almost cuboid at t=0 ns due to the initial system configuration, almost all methane molecules stay in the hydrate H-bonded cage except for that on the hydrate/water phase diffuse into the water phase. Subsequently, the hydrate cluster changes its shape from a rectangle to a core because the acute parts of the hydrate cluster between the silica walls dissociate faster than the planar parts due to the Gibbs−Thomson effect [76]. The manner of methane hydrate dissociation is stepwise, the inner layers decompose after the outer layers in a confined space constructed by two silica slabs, and this kinetics is very similar to that for hydrate dissociation without a presence of silica surface [38, 77]. The hydrate dissociation process is complicated, involving the collective motion of water and methane molecules [78]. Although the temperature of simulation system is higher than the hydrate equilibrium temperature, the existence of guest molecules can stabilize the hydrate cage [79, 80] and the inner hydrate phase can be preserved by the mass migration resistance compared with that at the interface layer where the dissociated fluid can be transported easily. Therefore, the hydrate phase dissociates from the outer to the inner in a stepwise manner (Limited by the configuration size and initial system temperature, there is no temperature gradient in the hydrate particle during its dissociation in our simulations (shown in Fig. S1)). Meanwhile, the residual hydrate cluster within the silica nanopore step-by-step dissociate in a shrinking core manner with a curved decomposition front until the thermal decomposition behavior is complete, which also observed in the Bagherzadeh's simulation [41].

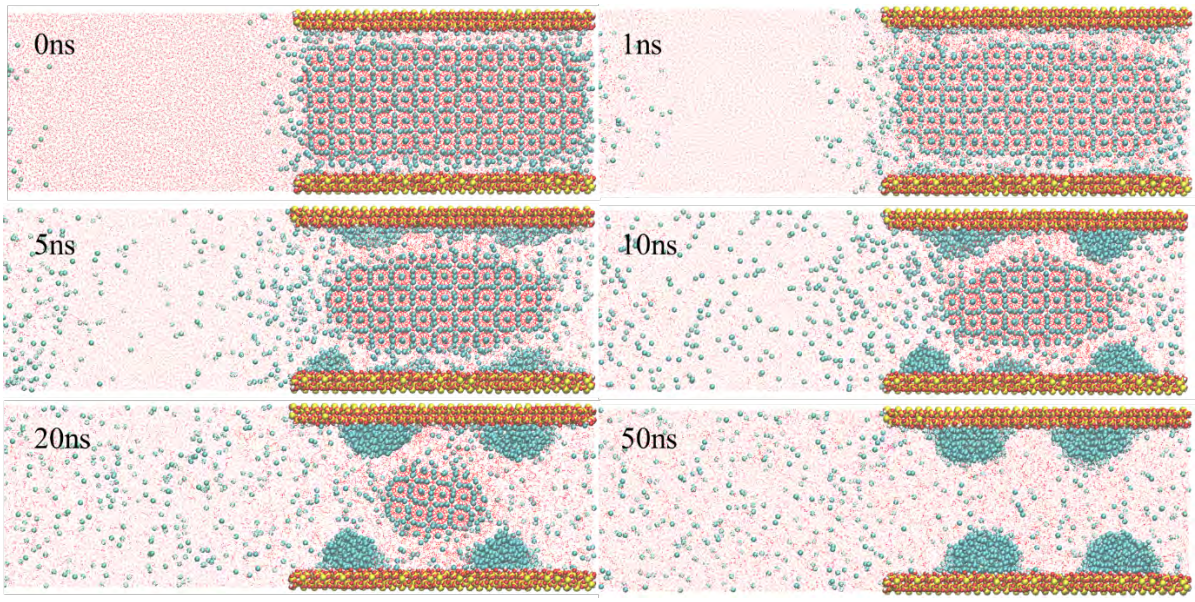

Fig. 2. Snapshots of the dissociation process of the hydrate cluster in the nanopore at initial temperature T = 292 K. Si (yellow); O (red); H (white); C (cyan). The evolution of hydrate phase and nanobubble can be observed clearly in those pictures.

The time variations of the temperature profiles of the entire simulation cell are shown in Fig. 3a. The average temperature in the NVE simulation drops as the simulations progress until the dissociation process is completed. This is because the decomposition of methane hydrates is an endothermic process. For the three simulations at initial temperatures of 292, 302 and 312 K, the dissociation processes continue for approximately 31.83, 8.98, and 2.85 ns, respectively, and the temperature drops for the three simulations are approximately 19.53, 17.1 and 12.8 K, respectively. In general, the dissociation process depends on the initial temperature of the reservoir, and the temperature drop is only related to the gas hydrate quantity. In our simulations, dissociation process of hydrate phase takes place during the equilibration period. Therefore, the quantity of undecomposed hydrate is different at the beginning of the NVE simulation at a series of initial temperatures. The higher the system temperature is, the faster the dissociation rate is, leading to less hydrate phase presence in the system (see Fig. S2). In the actual production, the utilized of depressurization technology to extract methane from hydrate occurring reservoirs is the most effective method. However, this method cannot supply the large amount of heat required for the endothermic reaction of hydrate decomposition. Fig. 3b indicates that the number of methane molecules belonging to the hydrate phase decrease due to the methane released during the dissociation process, and the number of unreleased methane profiles of the dissociation system are in accordance with the temperature profiles.

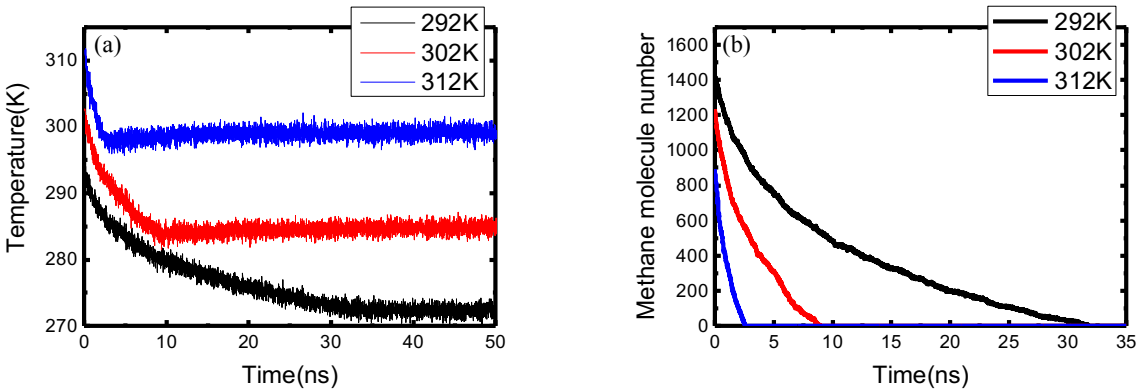

Fig. 3 Time evolution of the temperature profile (a) and the number of methane molecules remaining trapped in the hydrate phase (b). The legend is the simulation system initial temperature.

The number of methane molecules in the hydrate cluster at the different initial temperatures were fitted by an exponential decay function as follows:

$$N(t) = N_0 e^{-\alpha t} \qquad (2)$$

where N(t) and N_0 are the number of methane molecules corresponding to times t and 0, respectively, and α is the exponential decay time constant. The values of α are 0.11 ns^{-1}, 0.33 ns^{-1} and 1.04 ns^{-1} for the three simulations at initial temperatures of 292 K, 302 K, and 312 K, respectively. The hydrate dissociation rates occurring in the silica pores are obtained by taking the time derivative with respect to the number of methane molecules in the hydrate phase, as shown in Fig. 4. As expected, the rate of decomposition is not constant, as it is higher at a higher initial simulation temperature and at the beginning of the dissociation process. Over time, the rate decreases rapidly because the hydrate phase also decreases rapidly within the silica pore, and the higher the initial temperature is, the higher the rate of decrease is until the process is completed.

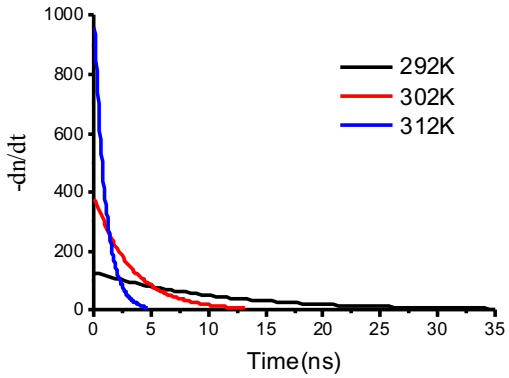

Fig. 4. Dissociation rate of the hydrate calculated by the negative derivative of the fitting equation (Eq 2) at a series of initial temperatures (292 K, 302 K and 312 K).

3.2 Evolution of the nanobubbles

As hydrate dissociation proceeds, methane molecules are released into the aqueous phase and the concentration of methane molecules in the vicinity of hydrate/water interface increases rapidly. Driven by the concentration gradient, methane molecules diffuse from hydrate block vicinity (high concentration) to bulk phase and water layer between silica slab and hydrate phase (both are with low concentration at initial simulation). When a significant amount of the hydrate block is dissociated, the diffusion rate of methane in the aqueous phase is less than the decomposition rate. Therefore, there is a local supersaturation of methane molecules, leading to gas molecules aggregation into a methane-rich region (nanobubble embryo) and phase separation between water and methane. The bubble embryos of methane molecules continue to grow as more of the hydrate is dissociated, eventually aggregate into clusters under this temperature-pressure condition. We identify these clusters as nanobubbles. Gas bubbles can be naturally generated or intentionally introduced in sediments, and it has been shown that this nanobubble formation, which presents a strong adsorption of methane in the aqueous phase, significantly affects the methane hydrate dissociation kinetics [74, 81]. Interestingly, the interfaces of the silica/water phase and hydrate/water phase in Fig. 2 and 5, respectively, indicate that methane molecules preferentially accumulate at this interface. Due to the Gibbs−Thomson effect [76], the acute parts of the hydrate cluster dissociate first (shown in Fig. 2), the methane molecules release from this part of the hydrate cage and adsorb on the silica surface [82]. Several factors may contribute to the formation of methane nanobubbles on hydrophilic silica surfaces. The first is that the adsorption behavior of CH_4 on the solid surface with silanol groups in CH_4-H_2O-SiO_2 three phase system is more complicated than CH_4-SiO_2 or H_2O-SiO_2 two phase systems; this process is affected by temperature, pressure and water content. Recently experimental work shows that at a certain water content, confined water molecules (water within the pores) can promoted the adsorption of CH_4 by forming deeper adsorption potential energy wells on hydrophilic silica surfaces, making the system more stable [83]. The simulation results by He et al. also show that methane nanobubbles can occur on the hydrophilic silica surface for a long time [56]. The second effect is that the kinetics factor may be important. During the decomposition of hydrates, methane molecules did not immediately release from the silica nanopore to the bulk phase, instead, they aggregate in the silica nanopore and form bubbles on the surface. The adsorption and confinement effects limit methane diffusion and facilitate methane aggregation upon the silica surfaces, eventually forming nanobubbles, which is quite different from dissociation without silica pores [48, 50, 84, 85]. The methane bubbles form to minimize the surface contacts of the methane molecules with water and hydrophilic hydroxylated silica surfaces. Yagasaki's work [74] shows that bubble formation can enhance the dissociation process. In our simulations, we also observed that the hydrate phase near the nanobubbles dissociates faster than that near the other surface area, as shown in Fig. 2.

The formation and migration of nanobubbles are strongly dependent on the temperature, in addition to the confinement space. We observed that nanobubbles formed on the hydroxylated silica surfaces, while nanobubbles also formed at the initial interface of the bulk/hydrate phase during dissociation at a relatively high initial temperature (302 K and 312 K), as shown in Fig. 5a. These results are caused by the different initial temperatures. The dissociation rate is excessively higher than the diffusion rate, and the bubble embryo formation in the vicinity of the hydrate/liquid interface at a higher temperature. Based on the MD simulations, the deformation and moving behaviors of the nanobubbles and the coalescence of the nanobubbles in the dissociation system can be directly observed. It is important to note that long simulation times lead to merging of the nanobubbles in this system. In our simulations, the nanobubble embryo formation in the initial vicinity of the hydrate/bulk interface moved with the fluid and merged with the larger nanobubble formation on the silica surface. In addition, the nanobubble formation and growth on silica also coalesced into a larger gas group, as shown in Fig. 5b. When the temperature of the system is high, the coalescence processes of nanobubbles will accelerate, which is why no coalescence process occurs at an initial temperature 292 K within the simulation time (Fig. 2).

During the evolution of the nanobubbles, hydrate methane molecules escape from the incomplete hydrate cages and dissolve in the surrounding water phase. In our simulations, methane molecules aggregate on the silica surface due to the adsorption and stereo-hindrance effects. Interestingly, the shapes of the nanobubbles aggregated on the silica surface do not reflect the hydrophobic properties of methane molecules, which may be caused by the confined space in the pore being occupied by the undecomposed hydrate phase. The bubbles of methane molecules continue to grow as more of the hydrate is dissociated. The nanobubbles transform to half cylinder-shaped bubbles due to the periodic boundary conditions, and hydrophobic properties are presented but are not completely satisfied, which may be caused by the extension of the silica crystal to decrease the mismatch between the silica.

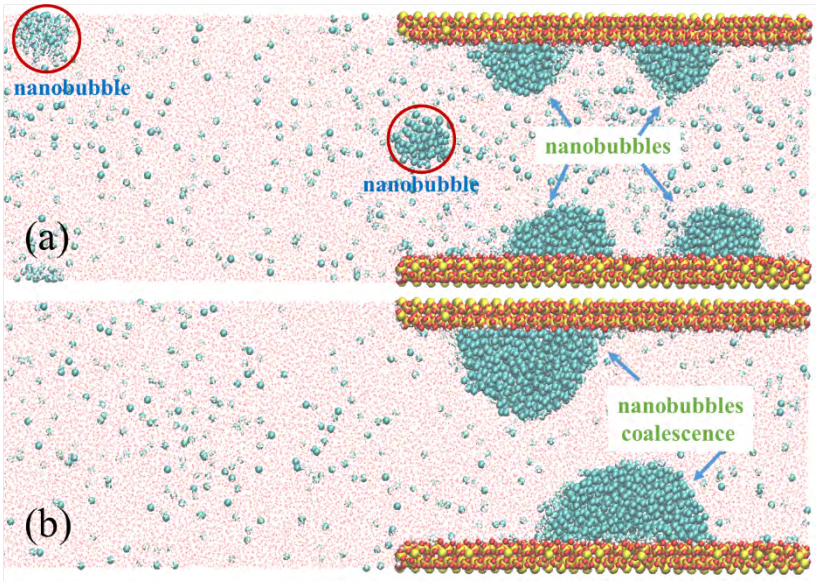

Fig. 5. Nanobubble evolution at a high initial temperature (302 K): time-lapse snapshots at 10 ns (a) and 50 ns (b). Si (yellow); O (red); H (white); C (cyan).

3.3 Gas/water migration

From an application point of view, the amount of methane that can be extracted from the sediments is important. In our simulations, the method of extraction is natural diffusion driven by molecular thermal motion and molecular concentration gradient. Thermal stimulation can be mainly implemented by the following manners: hot water or steam injection, microwave radiation, electrical heating,[3] with the purpose of rising the temperatures of local NGH reservoirs by heating. Once the local temperature increases above the phase equilibrium temperature at the local pressure, NGHs dissociate with the natural gas and water release. To quantify how much released methane gas has migrated to the water phase, the numbers of gas molecules in the different phases were counted, and the methane and water molecules from hydrate release into the bulk phase are counted, as shown in Fig. 6.

Higher simulation temperatures result in higher molecular kinetic energy levels that facilitate the migration of molecules. Based on the theory of molecular motion, the number of released methane and water molecules in the bulk phase diffused from the pore phase should be larger with increasing initial simulation temperature, whereas the simulation results shown in Fig. 6 do not completely agree with this deduction. Within the scope of the initial temperature and time, the deduction still applies for methane diffusion; however, when the initial temperature increases or as the dissociation process proceeds, the amount of released methane in the bulk phase decreases. This finding implied that the thermal stimulation of hydrate production from sediments can increase the dissociation rate within the range of the initial temperature, whereas gas production is an intricate process without depressurization; the number of released methane molecules in the bulk phase first increases rapidly and then decreases when the initial temperature is higher

than a certain value. In sharp contrast, the number of released water molecules increases as the growth rate slows as expected. The results are attributed to the kinetics of hydrate dissociation and the evolution of the nanobubbles of methane on the silica surfaces (formation, movement and mergence). At a high initial temperature, the dissociation rate is higher, nanobubble embryos are formed rapidly on the surface of the hydrate as well as the silica surfaces, as shown in Fig. 7. Then, the released methane molecules are adsorbed onto these nanobubble embryos, and the evolution of nanobubbles works against the gas molecules migrating out the nanopore. Under the effect of thermal movement, these nanobubbles are adsorbed and merge into large nanobubbles on the silica surface to decrease the surface energy, while the released water is free from the effect of the nanobubbles. Overall, thermal stimulation does not result in higher production from gas hydrates in low-permeability sediments if the methane molecules are not extracted immediately.

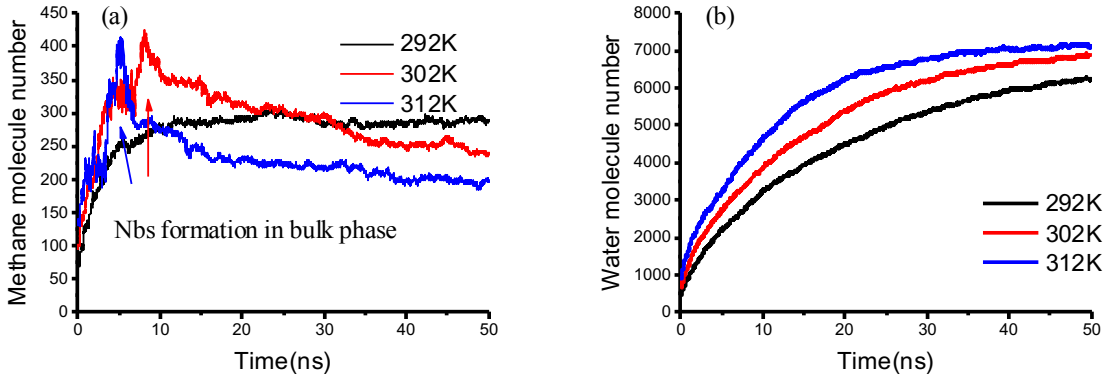

Fig. 6. The number of methane (a) and water (b) molecules in the bulk phase evolving with the simulation time; both molecules were released from the hydrate phase.

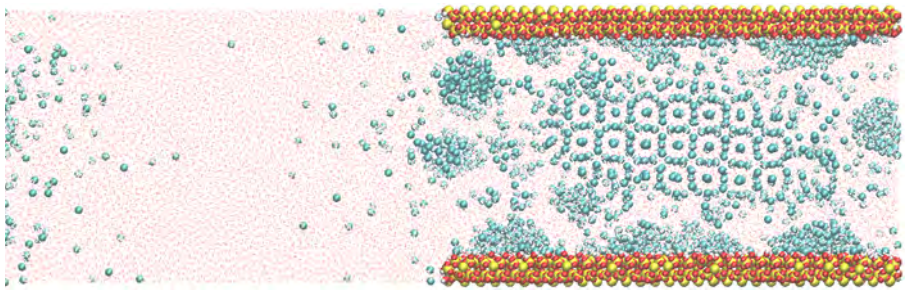

Fig. 7. Snapshot of the dissociation process at the 312 K initial temperature at 1 ns. Si (yellow); O (red); H (white); C (cyan).

4. Discussion

The capillary pressure is a function of the medium (geometry, interfacial tension and wettability) and the saturations of all phases (water, gas, hydrate) in the pore space. Previous studies have shown that the

water and gas flow can be greatly affected by capillary effects [86]. The capillary effects arising from the nano pore size can be attributed to the adsorption of methane and water molecules on the hydroxylated silica surface. For an approximate description of gas production from hydrates, the time evolution of the quantity of the released methane and water molecules from the hydrate phase in three phases (hydrate phase, silica pore phase and bulk phase) are shown in Fig. 8. The figure clearly shows that most of the released methane molecules remain in the pore phase, while in our simulations the released water molecules gradually diffuse to the bulk phase from the nanopore. As discussed above, the released methane molecules aggregate and gradually form nanobubbles, and the nanobubbles are always adsorbed on the silica surface. The adsorption is stable during the MD simulations unless there is an external disturbance or depressurization. The released gas molecules form nanobubbles inside the pore instead of entering the bulk phase, which is negative to the further methane production. At the same time, the nanobubbles also increase the pore pressure, even cause the excess pore pressure [87, 88], and affect the kinetics of dissociation in turn. In order to increase the gas production, some novel approaches should be proposed in NGH exploitation, for example, the inorganic small gas molecules (N_2, CO_2, H_2) injection method [89-91].

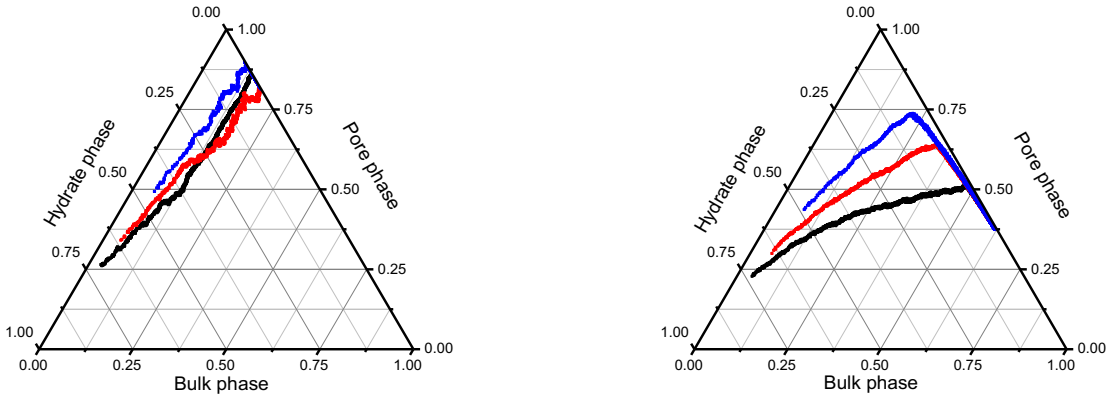

Fig. 8. Dissociated methane (a) and water (b) molecule distributions in the three phases (hydrate phase, silica pore phase and bulk phase) at the initial temperature of 292K (black), 302K (red), 312K (blue).

The simulations performed in this work are all in an adiabatic ensemble (NVE) which has no energy exchange with environment. As shown in Fig. 3(a), the endothermic reaction of hydrate decomposition reduces the amount of heat of the simulation systems, resulting in a large temperature drops before and after dissociation process. The heat consumption for this dynamics process can be replenished by the bulk water and silica phase in our simulations. At the field production condition, besides the latent heat of reservoirs, a continue heat supply by hot water or steam injection is necessary to sustain constant natural gas extraction form reservoirs. Therefore, the estimation of the rate of hot water supply is one of the important assurances for safe and effective production. Based on our simulation configuration, the rate of heat to be supplied is

equated to the rate of heat lost by the water phase (regarded as the hot water injection), which is given by the following equation.

$$\frac{m_{w0}C_{wV}(T_0-T_t)+m_{s0}C_{sV}(T_0-T_t)}{tV_h}=\frac{dm_{ws}}{dt}(T_0-T_{ref})C_V \quad (3)$$

where m_{w0} and m_{s0} are the initial mass of the water phase (including bulk phase and water layer between silica phase and hydrate phase) and silica phase respectively; m_{ws} represents the injection mass of the hot water to be supplied; C_{wV} and C_{sV} are the specific heat of water (taken as 84 J/(mol K) for the SPC/E water model[92]) and silica respectively; T_0 and T_t represent the initial temperature and temperature of at time *t* for the two phase; T_{ref} is the reference temperature (can be taken as 273 K), and V_h is the volume of the hydrate phase within the silica nanopore; *t* is the time.

Here, we suppose that the temperature of bulk phase is always the same as the silica phase during the simulations (silica atoms are free). The reduced heat can be calculated by equation Q=cmΔT (c is the specific heat; m is the mass; ΔT is the temperature gradient). Thus, we could calculate the heat loss to the two phases using this equation. The specific heat of water (taken as 4.19×10^3 J/(kg K) at 300 K[93]) is much larger than that of silica (7.45×10^2 J/(kg K) at 300 K[93]); and our configuration contains 22264 liquid water molecules including the bulk phase and two water buffer layers, the silica phase contains 5194 oxygen atoms, 2359 silicon atoms and 952 hydrogen atoms; the temperature gradient is the same. The heat loss of silica phase is about 6.7% to bulk phase. The heat loss of silica phase can be almost ignored, moreover, in our simulation the silica slabs were frozen during the simulation except the hydroxy group. Therefore, Eq 3 can be written as follow, and the equation is very similar to the Baghel's work [43].

$$\frac{m_{w0}C_V(T_0-T_t)}{tV_h}=\frac{dm_{ws}}{dt}(T_0-T_{ref})C_V \quad (4)$$

Since $m_{ws}=\rho_w V_{ws}$,

$$\frac{dV_{ws}}{dt}=\frac{m_{w0}(T_0-T_t)}{(T_0-T_{ref})tV_h\rho_w} \quad (5)$$

where ρ_w is the density of water and V_{ws} is the volume of water to be injected. The density of water was taken as 998 kg/m^3 for the SPC/E water model [94]. To extend the MD simulation results to the macroscopic scale, the time and space scale should be considered. As time variable is on both sides of Eq 5, the effect of the time scale is removed. Meanwhile, the heat supplied is directly proportional to the volume of hydrate in sediments, to remove the effect of the space scale, the rate of supply of hot water for a sustained dissociation process should be calculated per unit volume. The water phase temperature at time *t* (T_t) was equal to the average value of the last 100 data points of Fig. 3. Combined with the Eq 5 and digits from the simulations, the calculated values of the rate of supply of hot water at 292 K, 302 K and 312 K were 4.91×10^7 m^3/s m^3,

9.98×10^7 m^3/s m^3 and 1.75×10^8 m^3/s m^3, respectively. These results can represent the heat flow of the hydrate dissociation process in sediments, however, the calculation seems not so accurate because we lose sight of the latent heat of reservoirs. For example, the average porosity of hydrate reservoirs in Shenhu area of South China Sea is about 0.4 [95, 96], and the framework of the sediments accounted for 60%. Therefore, most of heat will be absorbed by the framework. However, in this work, the coordinates of silica atom were fixed except the OH group, resulting in the silica slab temperature almost unchanged. The heat supplement from sediment framework latent heat will be considered in our future work.

5. Conclusion

To investigate the dissociation kinetics closer to the sediment conditions of hydrate occurrences, methane hydrate dissociation in a confined space constructed by two fully hydroxylated silica surfaces that are ~80 Å apart with a bulk phase was simulated with MD at initial temperatures of 292, 302, and 312 K in an NVE ensemble. As expected, the rates of decomposition are low at low initial simulation temperatures. During hydrate dissociation, the undecomposed hydrate core shrank in a stepwise manner with a curved dissociation front. The evolution of methane nanobubbles in the presence of the silica surfaces was found to be quite different from that in nonconfined water methane hydrate simulations. The methane molecules released from the hydrate phase migrate to the aqueous phase and gather on the silica surface rapidly, leading to the formation of small nanobubbles and growth at a relatively low initial temperature (292 K). As the initial temperature increases, the rate of hydrate dissociation increases; thus, methane molecules rapidly assemble near the hydrate/bulk phase interface and on the silica surfaces, and the nanobubbles formed in the former merge into large nanobubbles on the silica surfaces over time to decrease the surface energy. More interestingly, the nanobubbles formed on the silica surfaces are not stable but also merge during the simulation process. As a result, a small portion of the released methane was found to actually enter the bulk phase (outside the pore phase) regardless of the initial temperature. In addition, although a high dissociation temperature environment can accelerate the process of decomposition, gas production does not always increase, and heat flow should be significantly supplied if thermal stimulation is used to produce gas from low-permeability hydrate reservoirs.

The present study reveals the remarkable confinement effect (caused by quartz sand intergranular nanopores) on the dissociation of methane hydrates. Thermal injection may enhance the hydrate dissociation process, but is independent of methane extraction; most of the dissociated methane molecules occur in the form of nanobubbles and are adsorbed on hydroxylated silica surfaces. It should be noticed that the simulations in this study were performed with respect to a static system. However, in the actual production

of gas hydrate resources, pressure differences are present, which can help the methane bubbles migrate from sandy sediments and contribute to the gas yields. Our future simulation work will be performed towards this direction.

Acknowledgment:

This work was supported by the China Geological Survey [DD20190232], Qingdao National Laboratory for Marine Science and Technology Open Fund [QNLM2016ORP0203 and MMRZZ201806], the National Key Research and Development Program of China [2017YFC0307600], the Fundamental Research Funds of the National University, China University of Geosciences (Wuhan) [CUGGC09,1810491T05], the National Natural Science Foundation of China [41672367,11772278]. The High Performance Computing Center of the CUG is acknowledged for providing computing resources.

[1] E.D.S. Jr, C.A. Koh, Clathrate Hydrates of Natural Gases, Crc Press, (2008).
[2] L.J. Florusse, C.J. Peters, J. Schoonman, K.C. Hester, C.A. Koh, S.F. Dec, K.N. Marsh, E.D. Sloan, Stable low-pressure hydrogen clusters stored in a binary clathrate hydrate, Science, 306 (2004) 469-471.
[3] X.S. Li, C.G. Xu, Y. Zhang, X.K. Ruan, G. Li, Y. Wang, Investigation into gas production from natural gas hydrate: A review, Appl Energ, 172 (2016) 286-322.
[4] E.D.S.a.C.A. Koh, Clathrate hydrates of natural gases, Taylor & Francis/CRC Press,, Boca Raton, Florida, 2008.
[5] R. Boswell, Is Gas Hydrate Energy Within Reach?, Science, 325 (2009) 957-958.
[6] X.S. Li, Y.J.I. Zhang, E.C. Research, Study on Dissociation Behaviors of Methane Hydrate in Porous Media Based on Experiments and Fractional Dimension Shrinking-Core Model, Industrial & Engineering Chemistry Research, 50 (2011) 8263-8271.
[7] Z. Yin, G.J. Moridis, R.C. Zheng, H.K. Tan, P.J.I. Linga, E.C. Research, Numerical analysis of experiments on thermally-induced dissociation of methane hydrates in porous media, Industrial & Engineering Chemistry Research, 57 (2018) 5776-5791.
[8] T.H. Kwon, G.C. Cho, J.C.J.G. Santamarina, Gas hydrate dissociation in sediments: Pressure-temperature evolution, Geochemistry, Geophysics, Geosystems, 9 (2008).
[9] L. Jensen, K. Thomsen, N. von Solms, S. Wierzchowski, M.R. Walsh, C.A. Koh, E.D. Sloan, D.T. Wu, A.K. Sum, Calculation of Liquid Water-Hydrate-Methane Vapor Phase Equilibria from Molecular Simulations, J Phys Chem B, 114 (2010) 5775-5782.
[10] M.M. Conde, C. Vega, Determining the three-phase coexistence line in methane hydrates using computer simulations, J Chem Phys, 133 (2010).
[11] M.M. Conde, C. Vega, C. McBride, E.G. Noya, R. Ramirez, L.M. Sese, Can gas hydrate structures be described using classical simulations?, J Chem Phys, 132 (2010).
[12] M. Khurana, Z.Y. Yin, P. Linga, A Review of Clathrate Hydrate Nucleation, Acs Sustain Chem Eng, 5 (2017) 11176-11203.
[13] M.R. Walsh, C.A. Koh, E.D. Sloan, A.K. Sum, D.T. Wu, Microsecond Simulations of Spontaneous Methane Hydrate Nucleation and Growth, Science, 326 (2009) 1095-1098.

[14] M.R. Walsh, G.T. Beckham, C.A. Koh, E.D. Sloan, D.T. Wu, A.K. Sum, Methane Hydrate Nucleation Rates from Molecular Dynamics Simulations: Effects of Aqueous Methane Concentration, Interfacial Curvature, and System Size, J Phys Chem C, 115 (2011) 21241-21248.
[15] L.C. Jacobson, W. Hujo, V. Molinero, Amorphous Precursors in the Nucleation of Clathrate Hydrates, J Am Chem Soc, 132 (2010) 11806-11811.
[16] L.C. Jacobson, V. Molinero, Can Amorphous Nuclei Grow Crystalline Clathrates? The Size and Crystallinity of Critical Clathrate Nuclei, J Am Chem Soc, 133 (2011) 6458-6463.
[17] P.G. Debenedetti, S. Sarupria, Hydrate Molecular Ballet, Science, 326 (2009) 1070-1071.
[18] C. Moon, P.C. Taylor, P.M. Rodger, Molecular dynamics study of gas hydrate formation, J Am Chem Soc, 125 (2003) 4706-4707.
[19] R. Radhakrishnan, B.L. Trout, A new approach for studying nucleation phenomena using molecular simulations: Application to CO_2 hydrate clathrates, J Chem Phys, 117 (2002) 1786-1796.
[20] B.C. Knott, V. Molinero, M.F. Doherty, B. Peters, Homogeneous Nucleation of Methane Hydrates: Unrealistic under Realistic Conditions, J Am Chem Soc, 134 (2012) 19544-19547.
[21] J. Vatamanu, P.G. Kusalik, Unusual crystalline and polycrystalline structures in methane hydrates, J Am Chem Soc, 128 (2006) 15588-15589.
[22] S. Liang, P.G. Kusalik, Crystal Growth Simulations of H_2S Hydrate, J Phys Chem B, 114 (2010) 9563-9571.
[23] Z.J. He, P. Linga, J.W. Jiang, What are the key factors governing the nucleation of CO_2 hydrate?, Phys Chem Chem Phys, 19 (2017) 15657-15661.
[24] Z.J. He, K.M. Gupta, P. Linga, J.W. Jiang, Molecular Insights into the Nucleation and Growth of CH4 and CO2 Mixed Hydrates from Microsecond Simulations, J Phys Chem C, 120 (2016) 25225-25236.
[25] N.J. English, J.S. Tse, Mechanisms for Thermal Conduction in Methane Hydrate, Phys Rev Lett, 103 (2009).
[26] B. Peters, N.E.R. Zimmermann, G.T. Beckham, J.W. Tester, B.L. Trout, Path Sampling Calculation of Methane Diffusivity in Natural Gas Hydrates from a Water-Vacancy Assisted Mechanism, J Am Chem Soc, 130 (2008) 17342-17350.
[27] D.A.G. Gualdron, P.B. Balbuena, Classical molecular dynamics of clathrate-methane-water-kinetic inhibitor composite systems, J Phys Chem C, 111 (2007) 15554-15564.
[28] M.T. Storr, P.C. Taylor, J.P. Monfort, P.M. Rodger, Kinetic inhibitor of hydrate crystallization, J Am Chem Soc, 126 (2004) 1569-1576.
[29] T. Yagasaki, M. Matsumoto, H. Tanaka, Adsorption Mechanism of Inhibitor and Guest Molecules on the Surface of Gas Hydrates, J Am Chem Soc, 137 (2015) 12079-12085.
[30] P.A. Oluwunmi, A.R. Finney, P.M. Rodger, Molecular dynamics screening for new kinetic inhibitors of methane hydrate, Can J Chem, 93 (2015) 1043-1049.
[31] S.A. Bagherzadeh, S. Alavi, J.A. Ripmeestera, P. Englezos, Why ice-binding type I antifreeze protein acts as a gas hydrate crystal inhibitor, Phys Chem Chem Phys, 17 (2015) 9984-9990.
[32] T. Yagasaki, M. Matsumoto, H. Tanaka, Adsorption of Kinetic Hydrate Inhibitors on Growing Surfaces: A Molecular Dynamics Study, J Phys Chem B, 122 (2018) 3396-3406.
[33] A. Phan, T. Bui, E. Acosta, P. Krishnamurthy, A. Striolo, Molecular mechanisms responsible for hydrate anti-agglomerant performance, Phys Chem Chem Phys, 18 (2016) 24859-24871.
[34] T. Bui, A. Phan, D. Monteiro, Q. Lan, M. Ceglio, E. Acosta, P. Krishnamurthy, A. StrioloD, Evidence of Structure-Performance Relation for Surfactants Used as Antiagglomerants for Hydrate Management, Langmuir, 33 (2017) 2263-2274.
[35] M.A. Bellucci, M.R. Walsh, B.L. Trout, Molecular Dynamics Analysis of Anti-Agglomerant Surface Adsorption in Natural Gas Hydrates, J Phys Chem C, 122 (2018) 2673-2683.
[36] A.A. Bertolazzo, P.M. Naullage, B. Peters, V. Molinero, The Clathrate-Water Interface Is Oleophilic, J Phys Chem Lett, 9 (2018) 3224-3231.
[37] F. Jimenez-Angeles, A. Firoozabadi, Hydrophobic Hydration and the Effect of NaCl Salt in the

Adsorption of Hydrocarbons and Surfactants on Clathrate Hydrates, Acs Central Sci, 4 (2018) 820-831.
[38] L.A. Baez, P. Clancy, Computer-Simulation of the Crystal-Growth and Dissolution of Natural-Gas Hydrates, International Conference on Natural Gas Hydrates, 715 (1994) 177-186.
[39] K. Yasuoka, S. Murakoshi, Molecular dynamics simulation of dissociation process for methane hydrate, Ann Ny Acad Sci, 912 (2000) 678-684.
[40] Y. Iwai, H. Nakamura, Y. Arai, Y. Shimoyama, Analysis of dissociation process for gas hydrates by molecular dynamics simulation, Mol Simulat, 36 (2010) 246-253.
[41] S.A. Bagherzadeh, P. Englezos, S. Alavi, J.A. Ripmeester, Molecular Modeling of the Dissociation of Methane Hydrate in Contact with a Silica Surface, J Phys Chem B, 116 (2012) 3188-3197.
[42] J.F. Xu, T.T. Gu, Z.N. Sun, X.D. Li, X.P. Wang, Molecular dynamics study on the dissociation of methane hydrate via inorganic salts, Mol Phys, 114 (2016) 34-43.
[43] V.S. Baghel, R. Kumar, S. Roy, Heat Transfer Calculations for Decomposition of Structure I Methane Hydrates by Molecular Dynamics Simulation, J Phys Chem C, 117 (2013) 12172-12182.
[44] M. Uddin, D. Coombe, Kinetics of CH4 and CO2 Hydrate Dissociation and Gas Bubble Evolution via MD Simulation, J Phys Chem A, 118 (2014) 1971-1988.
[45] S. Sarupria, P.G. Debenedetti, Molecular Dynamics Study of Carbon Dioxide Hydrate Dissociation, J Phys Chem A, 115 (2011) 6102-6111.
[46] H. Ji, D. Chen, Z. Chen, G.J.J.o.P.C.C. Wu, Molecular Dynamics Simulation of Methane Hydrate Formation and Dissociation in the Clay Pores With Fatty Acids, 122 (2017) acs.jpcc.7b08808.
[47] T. Yagasaki, M. Matsumoto, Y. Andoh, S. Okazaki, H. Tanaka, Dissociation of Methane Hydrate in Aqueous NaCl Solutions, J Phys Chem B, 118 (2014) 11797-11804.
[48] S.A. Bagherzadeh, S. Alavi, J.A. Ripmeester, P. Englezos, Evolution of methane during gas hydrate dissociation, Fluid Phase Equilibr, 358 (2013) 114-120.
[49] N.J. English, E.T. Clarke, Molecular dynamics study of CO_2 hydrate dissociation: Fluctuation-dissipation and non-equilibrium analysis, J Chem Phys, 139 (2013).
[50] T. Yagasaki, M. Matsumoto, Y. Andoh, S. Okazaki, H. Tanaka, Effect of Bubble Formation on the Dissociation of Methane Hydrate in Water: A Molecular Dynamics Study, J Phys Chem B, 118 (2014) 1900-1906.
[51] S.A. Bagherzadeh, S. Alavi, J. Ripmeester, P. Englezos, Formation of methane nano-bubbles during hydrate decomposition and their effect on hydrate growth, J Chem Phys, 142 (2015).
[52] N.J. English, G.M. Phelan, Molecular dynamics study of thermal-driven methane hydrate dissociation, J Chem Phys, 131 (2009).
[53] J. Kondori, S. Zendehboudi, L. James, New insights into methane hydrate dissociation: Utilization of molecular dynamics strategy, Fuel, 249 (2019) 264-276.
[54] S. Liang, D. Rozmanov, P.G. Kusalik, Crystal growth simulations of methane hydrates in the presence of silica surfaces, Phys Chem Chem Phys, 13 (2011) 19856-19864.
[55] D.S. Bai, G.J. Chen, X.R. Zhang, W.C. Wang, Microsecond Molecular Dynamics Simulations of the Kinetic Pathways of Gas Hydrate Formation from Solid Surfaces, Langmuir, 27 (2011) 5961-5967.
[56] Z. He, P. Linga, J. Jiang, CH4 Hydrate Formation between Silica and Graphite Surfaces: Insights from Microsecond Molecular Dynamics Simulations, Langmuir, 33 (2017) 11956-11967.
[57] D. Bai, G. Chen, X. Zhang, W. Wang, Nucleation of the CO2 hydrate from three-phase contact lines, Langmuir, 28 (2012) 7730-7736.
[58] D.S. Bai, G.J. Chen, X.R. Zhang, A.K. Sum, W.C. Wang, How Properties of Solid Surfaces Modulate the Nucleation of Gas Hydrate, Sci Rep-Uk, 5 (2015).
[59] S. Liang, P.G. Kusalik, The nucleation of gas hydrates near silica surfaces, Can J Chem, 93 (2015) 791-798.
[60] M. Chaouachi, A. Falenty, K. Sell, F. Enzmann, M. Kersten, D. Haberthur, W.F. Kuhs, Microstructural evolution of gas hydrates in sedimentary matrices observed with synchrotron X-ray computed tomographic microscopy, Geochem Geophy Geosy, 16 (2015) 1711-1722.

[61] B. Hess, C. Kutzner, D. van der Spoel, E. Lindahl, GROMACS 4: Algorithms for highly efficient, load-balanced, and scalable molecular simulation, J Chem Theory Comput, 4 (2008) 435-447.
[62] M.J. Abraham, T. Murtola, R. Schulz, S. Páll, J.C. Smith, B. Hess, E.J.S. Lindahl, GROMACS: High performance molecular simulations through multi-level parallelism from laptops to supercomputers, 1-2 (2015) 19-25.
[63] F. Takeuchi, M. Hiratsuka, R. Ohmura, S. Alavi, A.K. Sum, K. Yasuoka, Water proton configurations in structures I, II, and H clathrate hydrate unit cells, J Chem Phys, 138 (2013).
[64] R.T. Downs, M. Hall-Wallace, The American mineralogist crystal structure database, Am Mineral, 88 (2003) 247-250.
[65] M.G. Martin, J.I. Siepmann, Transferable potentials for phase equilibria. 1. United-atom description of n-alkanes, J Phys Chem B, 102 (1998) 2569-2577.
[66] H.J.C. Berendsen, J.R. Grigera, T.P. Straatsma, The missing term in effective pair potentials, The Journal of Physical Chemistry, 91 (1987) 6269-6271.
[67] P.E.M. Lopes, V. Murashov, M. Tazi, E. Demchuk, A.D. MacKerell, Development of an empirical force field for silica. Application to the quartz-water interface, J Phys Chem B, 110 (2006) 2782-2792.
[68] U. Essmann, L. Perera, M.L. Berkowitz, T. Darden, H. Lee, L.G. Pedersen, A Smooth Particle Mesh Ewald Method, J Chem Phys, 103 (1995) 8577-8593.
[69] M.A. Ratner, Understanding molecular simulation: From algorithms to applications, by Daan Frenkel and Berend Smit, Physics Today, 50 (1997) 66.
[70] K. Zimmermann, Oral - All Purpose Molecular Mechanics Simulator and Energy Minimizer, J Comput Chem, 12 (1991) 310-319.
[71] G. Bussi, D. Donadio, M. Parrinello, Canonical sampling through velocity rescaling, J Chem Phys, 126 (2007).
[72] M. Parrinello, Polymorphic transitions in single crystals: A new molecular dynamics method, J Appl Phys, 52 (1981) 7182-7190.
[73] M.J. Uttormark, M.O. Thompson, L.A. Baez, P. Clancy, Solid-Liquid Cluster Recognition in Heterogeneous Systems, Mol Simulat, 11 (1993) 121-144.
[74] Y. Takuma, M. Masakazu, A. Yoshimichi, O. Susumu, T. Hideki, Dissociation of methane hydrate in aqueous NaCl solutions, J Phys Chem B, 118 (2014) 11797-11804.
[75] T. Yagasaki, M. Matsumoto, Y. Andoh, S. Okazaki, H. Tanaka, Effect of bubble formation on the dissociation of methane hydrate in water: a molecular dynamics study, J Phys Chem B, 118 (2014) 1900-1906.
[76] C.A. Johnson, Generalization of the Gibbs-Thomson equation, Surf Sci, 3 (1965) 429-444.
[77] L.Y. Ding, C.Y. Geng, Y.H. Zhao, H. Wen, Molecular dynamics simulation on the dissociation process of methane hydrates, Mol Simulat, 33 (2007) 1005-1016.
[78] S. Liang, L.Z. Yi, D.Q. Liang, Molecular Insights into the Homogeneous Melting of Methane Hydrates, J Phys Chem C, 118 (2014) 28542-28547.
[79] E.M. Myshakin, H. Jiang, R.P. Warzinski, K.D. Jordan, Molecular Dynamics Simulations of Methane Hydrate Decomposition, J Phys Chem A, 113 (2009) 1913-1921.
[80] C. Windmeier, L.R. Oellrich, Theoretical Study of Gas Hydrate Decomposition Kinetics-Model Development, J Phys Chem A, 117 (2013) 10151-10161.
[81] T. Yagasaki, M. Matsumoto, Y. Andoh, S. Okazaki, H. Tanaka, Effect of bubble formation on the dissociation of methane hydrate in water: a molecular dynamics study, J Phys Chem B, 118 (2014) 1900.
[82] J.H. Weijs, J.H. Snoeijer, D.J.P.R.L. Lohse, Formation of surface nanobubbles and the universality of their contact angles: a molecular dynamics approach, 108 (2012) 104501.
[83] L. Wang, Q. Yu, Methane adsorption on porous nano-silica in the presence of water: An experimental and ab initio study, J Colloid Interface Sci, 467 (2016) 60-69.
[84] S. Alavi, J.A. Ripmeester, Nonequilibrium adiabatic molecular dynamics simulations of methane clathrate hydrate decomposition, J Chem Phys, 132 (2010) 144703.

[85] S.A. Bagherzadeh, P. Englezos, S. Alavi, J.A. Ripmeester, Molecular simulation of non-equilibrium methane hydrate decomposition process, J Chem Thermodyn, 44 (2012) 13-19.
[86] X.L. Liu, P.B. Flemings, Capillary effects on hydrate stability in marine sediments, J Geophys Res-Sol Ea, 116 (2011).
[87] W.Y. Xu, L.N. Germanovich, Excess pore pressure resulting from methane hydrate dissociation in marine sediments: A theoretical approach, J Geophys Res-Sol Ea, 111 (2006).
[88] Y. Sakamoto, T. Komai, T. Kawamura, H. Minagawa, N. Tenma, T. Yamaguchi, Laboratory-scale experiment of methane hydrate dissociation by hot-water injection and numerical analysis for permeability estimation in reservoir: Part 1 - Numerical study for estimation of permeability in methane hydrate reservoir, Int J Offshore Polar, 17 (2007) 47-56.
[89] Y.-F. Sun, J.-R. Zhong, R. Li, T. Zhu, X.-Y. Cao, G.-J. Chen, X.-H. Wang, L.-Y. Yang, C.-Y. Sun, Natural gas hydrate exploitation by CO2/H2 continuous Injection-Production mode, Appl Energ, 226 (2018) 10-21.
[90] X.-H. Wang, Y.-F. Sun, Y.-F. Wang, N. Li, C.-Y. Sun, G.-J. Chen, B. Liu, L.-Y. Yang, Gas production from hydrates by CH_4-CO_2/H_2 replacement, Appl Energ, 188 (2017) 305-314.
[91] D. Bai, X. Zhang, G. Chen, W. Wang, Replacement mechanism of methane hydrate with carbon dioxide from microsecond molecular dynamics simulations, Energy & Environmental Science, 5 (2012) 7033-7041.
[92] S.M. Park, P.H. Nguyen, G. Stock, Molecular dynamics simulation of cooling: Heat transfer from a photoexcited peptide to the solvent, J Chem Phys, 131 (2009).
[93] E.W. Lemmon, M.L. Huber, M.O.J.N.N.-. Mclinden, NIST Standard Reference Database 23: Reference Fluid Thermodynamic and Transport Properties-REFPROP, Version 9.1, (2010).
[94] P. Mark, L. Nilsson, Structure and dynamics of the TIP3P, SPC, and SPC/E water models at 298 K, J Phys Chem A, 105 (2001) 9954-9960.
[95] J.X. Sun, L. Zhang, F.L. Ning, H.W. Lei, T.L. Liu, G.W. Hu, H.L. Lu, J.A. Lu, C.L. Liu, G.S. Jiang, J.Q. Liang, N.Y. Wu, Production potential and stability of hydrate-bearing sediments at the site GMGS3-W19 in the South China Sea: A preliminary feasibility study, Mar Petrol Geol, 86 (2017) 447-473.
[96] J.X. Sun, F.L. Ning, H.W. Lei, X.R. Gai, M. Sanchez, J.G. Lu, Y.L. Li, L.L. Liu, C.L. Liu, N.Y. Wu, Y. He, M. Wu, Wellbore stability analysis during drilling through marine gas hydrate-bearing sediments in Shenhu area: A case study, J Petrol Sci Eng, 170 (2018) 345-367.

Supporting Information for

The Dynamic Behavior of Gas Hydrate Dissociation by Heating in Tight Sandy Reservoirs: A Molecular Dynamics Simulation Study

Bin Fang[1], Fulong Ning[1,2]*, Wenjia Ou[1], Dongdong Wang[1], Zhun Zhang[1,2], Yanjiang Yu[3], Hongfeng Lu[3], Jianyang Wu[4], Thijs J. H. Vlugt[5]

1 National Center for International Research on Deep Earth Drilling and Resource Development, Faculty of Engineering, China University of Geosciences, Wuhan, Hubei 430074, China

2 Laboratory for Marine Mineral Resources, Qingdao National Laboratory for Marine Science and Technology, Qingdao 266237, China

3 Guangzhou Marine Geological Survey, Ministry of Land and Resources, Guangzhou 510760, China

4 Department of Physics, Research Institute for Biomimetics and Soft Matter, Jiujiang Research Institute and Fujian Provincial Key Laboratory for Soft Functional Materials Research, Xiamen University, Xiamen 361005, PR China

5 Process and Energy Department, Delft University of Technology, Leeghwaterstraat 39, 2628CB Delft, The Netherlands

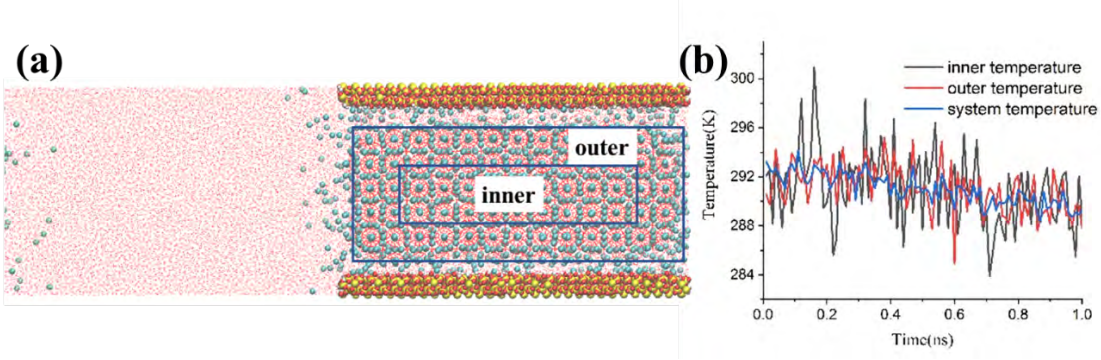

Fig. S1. We divided the hydrate phase into two parts: inner and outer. Subsequently, we calculated the temperature corresponding to the two parts as well as the simulation system (taken the case with the initial temperature 292K as an example). It shows that the temperature of the two parts is almost alike when the fluctuation is ignored.

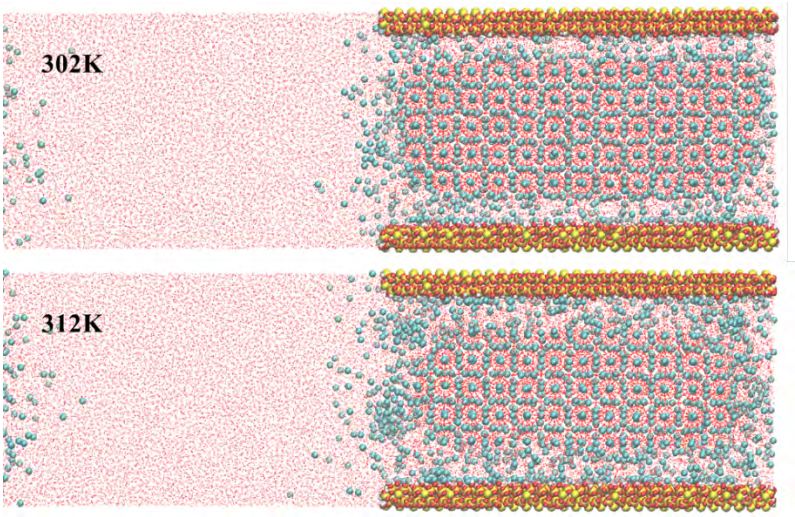

Fig. S2. Snapshots of the dissociation model after equilibrate simulation at the initial temperature of 302K and 312K.